LAWRENCE
LIVERMORE
NATIONAL
LABORATORY

UCRL-JRNL-206629

# Layzer type models for pressure driven shells

O. A. Hurricane

September 17, 2004

Physics of Fluids

# Layzer type models for pressure driven shells

O. A. Hurricane
*University of California, Lawrence Livermore National Laboratory*
*P.O. Box 808, Livermore, CA 94551*
*(UCRL-JRNL-??????, August 2004)*

Models for the nonlinear instability of finite thickness shells driven by pressure are constructed in the style of Layzer. Equations for both Cartesian and cylindrically convergent/divergent geometries are derived. The resulting equations are appropriate for incompressible shells with unity Atwood number. Predictions from the equations compare well with two-dimensional simulations.

PACS 53.35.Py, 47.20.Ky, 47.15.Hg

Instability theories for shells subject to a constant acceleration have been constructed for the linear case with arbitrary Atwood number [1] and nonlinear case with unity Atwood number [2] in Cartesian geometries. Although the importance of Rayleigh-Taylor (RT) instability to inertial confinement fusion (ICF) and astrophysical processes is quoted as the motivation for most works on RT theory, most of the physical instability drives encountered in ICF and astrophysics come from pressure ($P$) and not a constant acceleration ($g$).

A trivial substitution, $g \to P/\rho\Delta$ where $\rho$ is shell density and $\Delta$ is shell thickness, is generally not adequate since parts of the shell may accelerate relative to one another due to the shell thickness varying from location to location. The shell thickness variation may be imposed initially or my evolve as the instability proceeds. So, in order to resolve this effect a nonlinear theory for pressure driven shells is derived in this paper. The resulting equations will be limited to an incompressible shell with unity Atwood number, but results for both Cartesian and cylindrically convergent geometries will be obtained.

*Potential Flow Solution.* This method used here is based upon Layzer's [3] single interface treatment and its extension by Hecht *et al.* [2], so like these papers we will assume potential flow, i.e. the fluid velocity is, $\mathbf{v} = \boldsymbol{\nabla}\phi$ with $\phi$ being the velocity potential. If in addition we assume incompressible flow, then we know that $\phi$ must satisfy Laplaces equation $\nabla^2\phi = 0$.

Anywhere in the shell of fluid, the velocity potential must satisfy the Bernoulli equation

$$\frac{\partial\phi}{\partial t} + \frac{1}{2}\left|\nabla\phi\right|^2 + \frac{P}{\rho} = 0 \tag{1}$$

The above equation provides a moving boundary condition on both shell interfaces if the pressure is known on both shell interfaces. In particular, we will assume that the pressure at the upper shell interface boundary is known $P = \bar{P}$ which may be a function of time. At the lower shell boundary we assume $P = 0$.

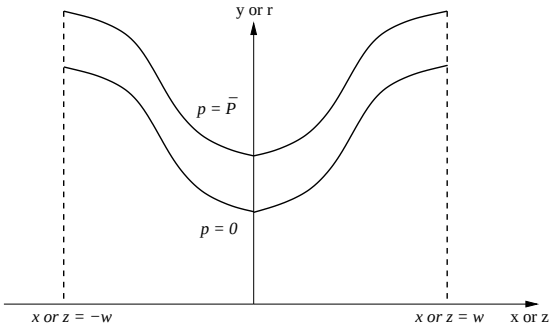


FIG. 1. A shell of material is driven from rest by a pressure $\bar{P}$. The notional flow of shell material is away from the bubble center at $x = 0$ towards the boundary (periodic or rigid) at $x = \pm w$.

The shape of the upper and lower shell interfaces are expressed as expansions in powers of $x$,

$$Y_t = \alpha_0(t) + \alpha_2(t)\,x^2 + \ldots \tag{2}$$
$$Y_b = \beta_0(t) + \beta_2(t)\,x^2 + \ldots \tag{3}$$

where the $\alpha$ and $\beta$ are time dependent coefficients that will be determined below. The initial value of the coefficients $\alpha$ and $\beta$ are determined from the initial imposed perturbation of the shell interfaces. The physical statement that the upper and lower liner interfaces move with the fluid is captured by the advective derivative equation

$$\frac{\partial Y}{\partial t} + \left.\frac{\partial\phi}{\partial x}\right|_Y \frac{\partial Y}{\partial x} - \left.\frac{\partial\phi}{\partial y}\right|_Y = 0 \tag{4}$$

which is evaluated at the upper and lower shell boundaries given by Eqs. [2,3]. Together, once we have a solution form for the velocity potential, Eqs. [1-4] completely determine the evolution of the shell.

*Cartesian Geometry.* In Cartesian geometry, the solution of the Laplace equation involves a Fourier series of exponential functions and trigonometric functions. Like Layzer, we only retain the first term of the Fourier sum in our solution

$$\phi = \left[a(t)e^{\frac{\pi y}{w}} + b(t)e^{\frac{-\pi y}{w}}\right]\cos\left(\frac{\pi x}{w}\right) + c(t)y + d(t) \tag{5}$$

where $a(t)$-$d(t)$ are time dependent coefficients that are to be determined. The only justification there is for dropping the higher terms in the Fourier solution comes from seeing that the above anzatz appears to give good results in the end.

The first few steps in the solution are somewhat mechanical, albeit the algebra is lengthy. We substitute Eq. [5] into Eq. [1] and then evaluate the result at the shell interfaces given by Eqs. [2,3] obtaining a complex expansion in even powers of $x$. Since the entire expression must evaluate to zero, we set coefficients of the expansion (which are functions of time only) to zero order-by-order. Thus at $\mathcal{O}(x^0)$ we find

$$\begin{aligned} \dot{a}e^{\frac{\pi\alpha_0}{w}} + \dot{b}e^{\frac{-\pi\alpha_0}{w}} + \dot{c}\alpha_0 + \dot{d} \\ +\frac{1}{2}\left[c\frac{\pi}{w}\left(ae^{\frac{\pi\alpha_0}{w}} - be^{\frac{-\pi\alpha_0}{w}}\right)\right]^2 + \frac{\bar{P}}{\rho} = 0 \end{aligned} \tag{6}$$

$$\begin{aligned} \dot{a}e^{\frac{\pi\beta_0}{w}} + \dot{b}e^{\frac{-\pi\beta_0}{w}} + \dot{c}\beta_0 + \dot{d} \\ +\frac{1}{2}\left[c\frac{\pi}{w}\left(ae^{\frac{\pi\beta_0}{w}} - be^{\frac{-\pi\beta_0}{w}}\right)\right]^2 = 0 \end{aligned} \tag{7}$$

where the over-dot stands for a time derivative. At $\mathcal{O}(x^2)$ we find

$$\begin{aligned} \frac{\pi}{w}\left(\alpha_2 - \frac{\pi}{2w}\right)\dot{a}e^{\frac{\pi\alpha_0}{w}} - \frac{\pi}{w}\left(\alpha_2 + \frac{\pi}{2w}\right)\dot{b}e^{\frac{-\pi\alpha_0}{w}} + \alpha_2\dot{c} \\ +\frac{\pi^2}{2w^2}\left(ae^{\frac{\pi\alpha_0}{w}} + be^{\frac{-\pi\alpha_0}{w}}\right)^2 \\ +\frac{\pi^2}{w^2}\left(\frac{\pi a}{w}e^{\frac{\pi\alpha_0}{w}} - \frac{\pi b}{w}e^{\frac{-\pi\alpha_0}{w}} + c\right) \\ \times\left[\left(\alpha_2 - \frac{\pi}{2w}\right)ae^{\frac{\pi\alpha_0}{w}} + \left(\alpha_2 + \frac{\pi}{2w}be^{\frac{-\pi\alpha_0}{w}}\right)\right] = 0 \end{aligned} \tag{8}$$

and

$$\begin{aligned} \frac{\pi}{w}\left(\beta_2 - \frac{\pi}{2w}\right)\dot{a}e^{\frac{\pi\beta_0}{w}} - \frac{\pi}{w}\left(\beta_2 + \frac{\pi}{2w}\right)\dot{b}e^{\frac{-\pi\beta_0}{w}} + \beta_2\dot{c} \\ +\frac{\pi^2}{2w^2}\left(ae^{\frac{\pi\beta_0}{w}} + be^{\frac{-\pi\beta_0}{w}}\right)^2 \\ +\frac{\pi^2}{w^2}\left(\frac{\pi a}{w}e^{\frac{\pi\beta_0}{w}} - \frac{\pi b}{w}e^{\frac{-\pi\beta_0}{w}} + c\right) \\ \times\left[\left(\beta_2 - \frac{\pi}{2w}\right)ae^{\frac{\pi\beta_0}{w}} + \left(\beta_2 + \frac{\pi}{2w}be^{\frac{-\pi\beta_0}{w}}\right)\right] = 0 \end{aligned} \tag{9}$$

Similarly to the above, when we substitute Eq. [5] into Eq. [4] and then evaluate the results at the interfaces given by Eqs. [2,3] we obtain four more equations that close the system again by collecting terms in powers of $x$ and evaluating the coefficients to zero. Thus, we obtain at $\mathcal{O}(x^0)$

$$\dot{\alpha}_0 + \frac{\pi}{w}\left(ae^{\frac{\pi\alpha_0}{w}} + be^{\frac{-\pi\alpha_0}{w}}\right) - c = 0 \tag{10}$$

$$\dot{\beta}_0 + \frac{\pi}{w}\left(ae^{\frac{\pi\beta_0}{w}} + be^{\frac{-\pi\beta_0}{w}}\right) - c = 0 \tag{11}$$

while at $\mathcal{O}(x^2)$ we obtain

$$\begin{aligned} \dot{\alpha}_2 - \frac{3\pi^2}{w^2}\left(ae^{\frac{\pi\alpha_0}{w}} + be^{\frac{-\pi\alpha_0}{w}}\right)\alpha_2 \\ \frac{\pi^3}{2w^3}\left(ae^{\frac{\pi\alpha_0}{w}} - be^{\frac{-\pi\alpha_0}{w}}\right) = 0 \end{aligned} \tag{12}$$

$$\begin{aligned} \dot{\beta}_2 - \frac{3\pi^2}{w^2}\left(ae^{\frac{\pi\beta_0}{w}} + be^{\frac{-\pi\beta_0}{w}}\right)\beta_2 \\ \frac{\pi^3}{2w^3}\left(ae^{\frac{\pi\beta_0}{w}} - be^{\frac{-\pi\beta_0}{w}}\right) = 0 \end{aligned} \tag{13}$$

Eqs. [6-13] are completely closed and, with initial conditions, completely describe the evolution of the flow field and shell motion in the vicinity of the apex of the bubble. Although the equations are highly nonlinear, they are linear in terms of the time derivatives of the unknowns $a(t)$ to $d(t)$, the $\alpha$'s and the $\beta$'s. Eqs. [10-13] already have the time derivative isolated from the rest of the equation. For Eqs. [6-9] one may use standard matrix techniques to solve for the flow variables $a(t)$ to $d(t)$. One may reduce the complexity of the ultimate solution by eliminating the physically uninteresting quantity $\dot{d(t)}$ from Eqs. [6] and [7] by subtracting the two equations. One is left to solve a $3 \times 3$ system for $a$, $b$, and $c$.

*Cylindrical Geometry.* The solution for cylindrical geometry is similar to the Cartesian case, one difference is the form for $\phi$ that satisfies the Laplace equation

$$\begin{aligned} \phi = \left[a(t)I_0\left(\frac{\pi r}{w}\right) + b(t)K_0\left(\frac{\pi r}{w}\right)\right]\cos\left(\frac{\pi z}{w}\right) \\ +c(t)\ln\left(\frac{r}{w}\right) + d(t) \end{aligned} \tag{14}$$

Here the modified Bessel functions take the place of the exponentials used in the Cartesian case. Eq. [14] includes the effects of convergence (or alternatively divergence) through the modified Bessel functions. The second difference is a minor re-expression of the interface shapes in terms of $R$ and $z$, i.e. $R_t = \alpha_0(t) + \alpha_2(t)\,z^2 + \ldots$ and $R_b = \beta_0(t) + \beta_2(t)\,z^2 + \ldots$.

Otherwise the mathematical procedure is the same as the Cartesian case. Thus from Eq. [1] at $\mathcal{O}(z^0)$ we find

$$\begin{aligned} \dot{a}I_0\left(\frac{\pi\alpha_0}{w}\right) + \dot{b}K_0\left(\frac{\pi\alpha_0}{w}\right) + \dot{c}\ln\left(\frac{\alpha_0}{w}\right) + \dot{d} \\ +\frac{1}{2}\left[\frac{c}{\alpha_0} + \frac{\pi a}{w}I_1\left(\frac{\pi\alpha_0}{w}\right) - \frac{\pi b}{w}K_1\left(\frac{\pi\alpha_0}{w}\right)\right]^2 + \frac{\bar{P}}{\rho} = 0 \end{aligned} \tag{15}$$

$$\begin{aligned} \dot{a}I_0\left(\frac{\pi\beta_0}{w}\right) + \dot{b}K_0\left(\frac{\pi\beta_0}{w}\right) + \dot{c}\ln\left(\frac{\beta_0}{w}\right) + \dot{d} \\ +\frac{1}{2}\left[\frac{c}{\beta_0} + \frac{\pi a}{w}I_1\left(\frac{\pi\beta_0}{w}\right) - \frac{\pi b}{w}K_1\left(\frac{\pi\beta_0}{w}\right)\right]^2 = 0 \end{aligned} \tag{16}$$

At $\mathcal{O}(z^2)$ we find

$$\begin{aligned} \dot{a}\frac{\pi}{w}\left[\alpha_2 I_1\left(\frac{\pi\alpha_0}{w}\right) - \frac{\pi}{2w}I_0\left(\frac{\pi\alpha_0}{w}\right)\right] \\ -\dot{b}\frac{\pi}{w}\left[\alpha_2 K_1\left(\frac{\pi\alpha_0}{w}\right) + \frac{\pi}{2w}K_0\left(\frac{\pi\alpha_0}{w}\right)\right] \\ +\dot{c}\frac{\alpha_2}{\alpha_0} + \frac{\pi^4}{2w^4}\left[aI_0\left(\frac{\pi\alpha_0}{w}\right) + bK_0\left(\frac{\pi\alpha_0}{w}\right)\right]^2 \end{aligned}$$

$$+\left[\frac{c}{\alpha_0}+\frac{\pi a}{w}I_1\left(\frac{\pi\alpha_0}{w}\right)-\frac{\pi b}{w}K_1\left(\frac{\pi\alpha_0}{w}\right)\right]$$
$$\times\left\{\frac{\pi^2\alpha_2 a}{2w^2}\left[I_2\left(\frac{\pi\alpha_0}{w}\right)+I_0\left(\frac{\pi\alpha_0}{w}\right)\right]\right.$$
$$-\frac{\pi^3 a}{2w^3}I_1\left(\frac{\pi\alpha_0}{w}\right)+\frac{\pi^2\alpha_2 b}{2w^2}\left[K_2\left(\frac{\pi\alpha_0}{w}\right)+K_0\left(\frac{\pi\alpha_0}{w}\right)\right]$$
$$\left.-\frac{\pi^3 b}{2w^3}K_1\left(\frac{\pi\alpha_0}{w}\right)-c\frac{\alpha_2}{\alpha_0}\right\}=0 \quad (17)$$

and

$$\dot{a}\frac{\pi}{w}\left[\beta_2 I_1\left(\frac{\pi\beta_0}{w}\right)-\frac{\pi}{2w}I_0\left(\frac{\pi\beta_0}{w}\right)\right]$$
$$-\dot{b}\frac{\pi}{w}\left[\beta_2 K_1\left(\frac{\pi\beta_0}{w}\right)+\frac{\pi}{2w}K_0\left(\frac{\pi\beta_0}{w}\right)\right]$$
$$+\dot{c}\frac{\beta_2}{\beta_0}+\frac{\pi^4}{2w^4}\left[aI_0\left(\frac{\pi\beta_0}{w}\right)+bK_0\left(\frac{\pi\beta_0}{w}\right)\right]^2$$
$$+\left[\frac{c}{\beta_0}+\frac{\pi a}{w}I_1\left(\frac{\pi\beta_0}{w}\right)-\frac{\pi b}{w}K_1\left(\frac{\pi\beta_0}{w}\right)\right]$$
$$\times\left\{\frac{\pi^2\beta_2 a}{2w^2}\left[I_2\left(\frac{\pi\beta_0}{w}\right)+I_0\left(\frac{\pi\beta_0}{w}\right)\right]\right.$$
$$-\frac{\pi^3 a}{2w^3}I_1\left(\frac{\pi\beta_0}{w}\right)+\frac{\pi^2\beta_2 b}{2w^2}\left[K_2\left(\frac{\pi\beta_0}{w}\right)+K_0\left(\frac{\pi\beta_0}{w}\right)\right]$$
$$\left.-\frac{\pi^3 b}{2w^3}K_1\left(\frac{\pi\beta_0}{w}\right)-c\frac{\beta_2}{\beta_0}\right\}=0 \quad (18)$$

The equations coming from Eq. [4] are much simpler. At $\mathcal{O}(z^0)$ we have

$$\dot{\alpha}_0-\frac{\pi}{w}\left[aI_1\left(\frac{\pi\alpha_0}{w}\right)-bK_1\left(\frac{\pi\alpha_0}{w}\right)\right]-\frac{c}{\alpha_0}=0 \quad (19)$$

$$\dot{\beta}_0-\frac{\pi}{w}\left[aI_1\left(\frac{\pi\beta_0}{w}\right)-bK_1\left(\frac{\pi\beta_0}{w}\right)\right]-\frac{c}{\beta_0}=0 \quad (20)$$

Finally at $\mathcal{O}(z^2)$,

$$\dot{\alpha_2}-\alpha_2\left\{\frac{\pi^2 a}{2w^2}\left[I_2\left(\frac{\pi\alpha_0}{w}\right)+I_0\left(\frac{\pi\alpha_0}{w}\right)\right]\right.$$
$$+\frac{2\pi a}{w^2}I_0\left(\frac{\pi\alpha_0}{w}\right)+\frac{\pi^2 b}{2w^2}\left[K_2\left(\frac{\pi\alpha_0}{w}\right)+K_0\left(\frac{\pi\alpha_0}{w}\right)\right]$$
$$\left.+\frac{2\pi b}{w^2}K_0\left(\frac{\pi\alpha_0}{w}\right)-\frac{c}{\alpha_0^2}\right\}$$
$$+\frac{\pi^3}{2w^3}\left[aI_1\left(\frac{\pi\alpha_0}{w}\right)-bK_1\left(\frac{\pi\alpha_0}{w}\right)\right]=0 \quad (21)$$

and

$$\dot{\beta_2}-\beta_2\left\{\frac{\pi^2 a}{2w^2}\left[I_2\left(\frac{\pi\beta_0}{w}\right)+I_0\left(\frac{\pi\beta_0}{w}\right)\right]\right.$$
$$+\frac{2\pi a}{w^2}I_0\left(\frac{\pi\beta_0}{w}\right)+\frac{\pi^2 b}{2w^2}\left[K_2\left(\frac{\pi\beta_0}{w}\right)+K_0\left(\frac{\pi\beta_0}{w}\right)\right]$$
$$\left.+\frac{2\pi b}{w^2}K_0\left(\frac{\pi\beta_0}{w}\right)-\frac{c}{\beta_0^2}\right\}$$
$$+\frac{\pi^3}{2w^3}\left[aI_1\left(\frac{\pi\beta_0}{w}\right)-bK_1\left(\frac{\pi\beta_0}{w}\right)\right]=0 \quad (22)$$

Like the equations for the Cartesian case, these complex nonlinear equations are linear in terms of the time derivatives and can be inverted for the time derivatives using standard matrix techniques.

*Comparison with Simulation.* As a test of our equations, we compare the predictions of the equations presented in the previous section with the predictions of a direct simulation. The code we choose to use is CALE, which is a C-based arbitrary Lagrangian-Eulerian numerical scheme. We force CALE to run in pure Lagrangian mode so that the pressure boundary conditions match those we stated in the previous section. The simulations used a 91 × 91 resolution grid, with thirty zones used to resolve the shell thickness. Since CALE is actually a compressible hydrodynamics code, we take the equations of state to be ideal gases, but with polytropic indicies of $\gamma = 100$ in order to mimic an incompressible fluid, again to match the assumptions made in the theoretical development.

The initial shape of the shell interfaces for this example problem are given by Eqs. [2] and [3] with $\alpha_0 = 10.0$, $\beta_0 = 9.0$, and $\alpha_2 = 0.3$ and $\beta_2 = 0.1$. The pressure driving the bubble is taken to be $\bar{P} = 1$, the density of the shell is taken to be $\rho = 1$, and $w = 5$.

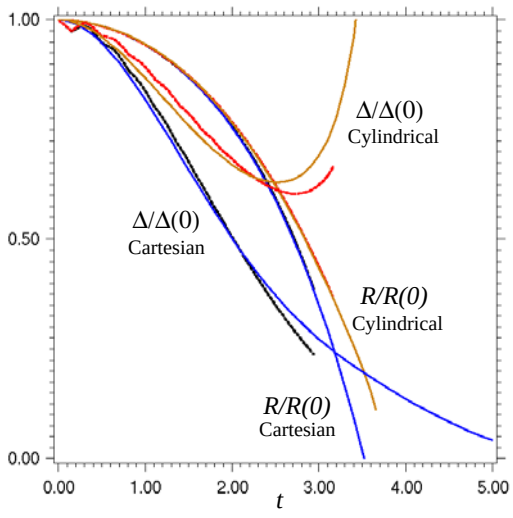


FIG. 2. A comparison of the position of the shell centroid, $R(t) = [\alpha_0(t) + \beta_0(t)]/2$, and shell thickness, $\Delta(t) = \alpha_0(t) - \beta_0(t)$, are shown for the Cartesian and cylindrical case. Both quantities are normalized to their initial values. The solid curves are from the simulation and the dotted curves are from the theory. The effects of convergence on $\Delta$ are obvious.

Fig. 2 compares the theoretical prediction of the bubble trajectory $R(t) = [\alpha_0(t)+\beta_0(t)]/2$ and the shell thickness $\Delta(t) = \alpha_0(t) - \beta_0(t)$ with those predicted by the simulation. The agreement is good until late time when the theory begins to underpredict the shell thinning when

compared to the simulation. The curves for $R(t)$ are in such good agreement that they are indistinguishable in the figure. The agreement for the bubble thickness is almost as good except for the small sound wave oscillation seen in the simulation results. Good agreement is also seen in the shell velocity as can be observed from Fig. 3.

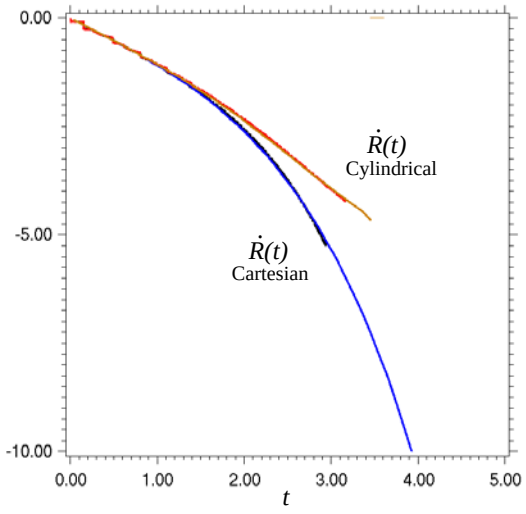


FIG. 3. The shell velocities, $\dot{R}(t)$, are intercompared between the simulation and theory for both the Cartesian and cylindrical cases. Not suprisingly, the shell in Cartesian geometry accelerates more rapidly than the cylindrical version.

*Feedthrough.* Classically from linear theory, the expected coupling strength between the two shell interfaces is expected to go as $\exp(-2\pi\Delta/w)$, e.g. Refs. [1] and [4], so it is not suprising to see that the cylindrical shell exhibits less coupling between the curvature of the interfaces than the Cartesian shell exhibits (see Fig. 4) even in the nonlinear phase. The natural thickening of the shell in the cylindrical case, due to convergence, pushes the interfaces apart and thus tends towards decoupling them. On the other hand, the tendancy of the Cartesian shell to continue to thin makes the instability feedthough and coupling of the interfaces inevitable.

*Conclusion.* We have developed a set of equations describing the nonlinear instability of pressure driven shells in both Cartesian and cylindrically convergent geometries. The analysis, based upon the original work of Layzer [Ref. [3]], appears to work fairly well at describing the evolution of the bubble apex even in convergent geometry. The model appears to accurately predict the shell trajectory and velocity when compared to simulation and to a lesser extent predicts shell thickness changes. Unlike constant acceleration models of unstable shells, the present model includes the effect of changing acceleration in response to shell thickness evolution–a condition more relevant to inertial confinment fusion.

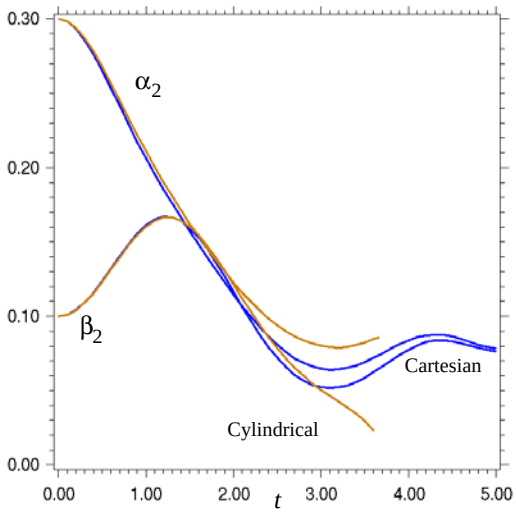


FIG. 4. The parameters related to bubble curvature, $\alpha_2(t)$ and $\beta_2(t)$, are shown as the models for the Cartesian and cylindrical shells are evolved. A decreasing $\alpha_2$ or $\beta_2$ parameter indicates flattening. The Cartesian shell shows much more correlation between the curvature of the upper and lower interface than the cylindrical case shows. The Cartesian shell also shows an oscillation in the interface curvature that is not seen in the cylindrical version.

## ACKNOWLEDGMENTS

This work was motivated by discussions with Dr's. James H. Hammer, Mark C. Herrmann, and Daniel S. Clark. This work was performed under the auspices of the U.S. Department of Energy by the University of California Lawrence Livermore National Laboratory under contract No. W-7405-Eng-48.

[1] K. O. Mikaelian, "Rayleigh-Taylor and Richtmyer-Meshkov instabilities in finite-thickness fluid layers," Phys. Fluids, **7**, 888 (1995).

[2] J. Hecht, U. Alon, and D. Shvarts, "Potential flow models of Rayleigh-Taylor and Richtmyer-Meshkov bubble fronts," Phys. Fluids, **6**, 4019 (1994).

[3] D. Layzer, "On the gravitational instability of two superposed fluids in a gravitational field," Astrophys. J., **122**, 1 (1955).

[4] G. I. Taylor, "The instability of liquid surfaces when accelerated in a direction perpendicular to their planes, I," Proc. R. Soc. London Ser. A, **201**, 192 (1950).